Suppression of Large Scale Structures in a Turbulent von Kármán Flow using Random Forcing

Hanna Berning, Tim Grünberg and Thomas Rösgen

Institute of Fluid Dynamics
ETH Zurich
8092 Zurich, Switzerland
berning@ifd.mavt.ethz.ch

ABSTRACT

Low wavenumber instabilities in a von Kármán flow cell are significantly reduced in an experiment by applying a variable forcing. By reversing the disc rotation sense pseudo-randomly or regularly, only the poloidal inward pumping remains at sufficiently high change rates. We investigate the influence of the forcing on the macroscopic scale with ultrasound Doppler measurements along a line in the transversal plane of the cell. The suppression of slow, persistent instabilities throughout the cell results in a cut-off of low wavenumber modes in the velocity spectrum and decreasing characteristic autocorrelation times. Turbulence properties are further examined in the center of the cell by temporally and spatially resolved Lagrangian ultrasound particle tracking. Turbulence features such as peak height of the compensated second order structure functions or higher order moments of the velocity fluctuations remain as expected for a fully turbulent flow. With only the poloidal base flow mode remaining, this forcing method allows to investigate turbulence phenomena in the center of the cell without superimposed effects.

INTRODUCTION

For turbulence research, it is desirable to create a highly turbulent flow in confined geometries. A standard approach is the use of two counter-rotating discs in a cylinder, creating the von Kármán flow (Douady et al., 1991; Maurer et al., 1994; Voth et al., 2002). Unfortunately, this flow exhibits a multiplicity of complex instabilities which are very sensitive to boundary conditions - e.g. aspect ratio (Nore et al., 2004) or blade shape (Ravelet et al., 2004) - and energy injection mechanisms - e.g. rotation frequency or asymmetry (Saint-Michel et al., 2014; Cortet et al., 2009).

Several authors observed slow global multi-stabilities of the flow for a range of Reynolds numbers. De la Torre and Burguete (2007) found for a set-up with curved blades that the azimuthal velocity in the transversal plane experiences inversions above Re = 10^4 with time scales much larger than the period of the propeller. Grünberg and Rösgen (2016) and Miralles (2013) studied long-term stationary flow modes for straight blades and their stabilization in favor of one mode. Modifications which led to stabilization were introduced by means of anisotropy at the small scales via the directional alignment of paramagnetic nano chains in the former case. In the latter case these modes were enhanced by an external magnetic field in a magneto-hydrodynamic flow of a conductive fluid. The global modes might originate from persistent Kelvin-Helmholtz like vortices which were, among others, visualized by Cortet et al. (2009) in a cell with curved blades.

The occurrence of such flow patterns affects the homogeneity and isotropy of the flow. It is thus desirable to investigate modifications of the turbulent flow independent of these largest scale instabilities. Since the flow patterns are not yet fully understood and are unlikely to be controllable in a selective manner, we propose a method of suppressing the global, long-term modes in order to decrease their signature on turbulence properties in the center of the cell. This will be induced only by a variation of the boundary conditions, i.e. the forcing method, of the flow cell itself, such that it can be applied to any fluid. This way, magneto-hydrodynamic effects or other globally applied changes in fluid properties can be investigated independently.

Several authors already investigated different forcing types as compared to the steady forcing for counter-rotating discs. Cortet et al. (2009) and Saint-Michel et al. (2014) studied global bifurcations resulting from asymmetric disc frequencies. In addition, Saint-Michel et al. (2014) found hysteretic behavior for blades driven with constant torque and variable frequency. In a set-up where turbulence is created via the oscillation of two grids, Chien et al. (2013) used variable frequencies to drive the grids. In contrast to our work, they aimed at increasing the signature of the large-scale input onto the small scales. To our knowledge, it has not yet been tried to suppress these slow instabilities while retaining or improving the turbulence characteristics in the center of the cell.

We propose forcing with constant amplitude but random sense of rotation such that the establishment of long-term instabilities is inhibited. We apply a pseudo-random binary sequence (PRBS) which has the advantage of not introducing any particular spectral signature by deterministically approximating the spectrum of white noise. In order to investigate the dependence on the time scale of direction change, periodic direction changes are investigated as well using a regular square wave signal (SW). We choose a square wave signal as opposed to a harmonic signal in order to keep the forcing amplitude constant while maximizing the energy input into the system.

EXPERIMENTAL SET-UP

The experimental apparatus consists of the flow cell with two counter-rotating discs with eight straight blades each, driven by two brushless motors (figure 1). The fluid, water, is temperature controlled by cooling loops embedded in the top and bottom plates of the cylinder. The temperature is measured in the central plane of the cell and is held stable to within 0.1K throughout the tests. The speed of the upper and lower disc is the same, leading to a symmetric mean flow profile with respect to the transversal plane. All rotation sequences are driven with the same maximum angular velocity, resulting in a maximum Reynolds number of $\mathrm{Re}_{\mathrm{max}} = 47\,000$ or microscale Reynolds numbers Re_λ between 175 and 225. Some experimental parameters and their definitions are summarized in table 1, more details about the apparatus can be found in Grünberg and Rösgen (2016).

Since the current measurements in water will later be extended to an opaque ferrofluid, the flow is investigated both with a Eulerian and a Lagrangian ultrasound measurement technique.

The Eulerian measurements are carried out using an Ultrasound Doppler Velocity Profiler UDOP4000 (UDV) by Signal Processing SA which is able to quasi-simultaneously measure velocity

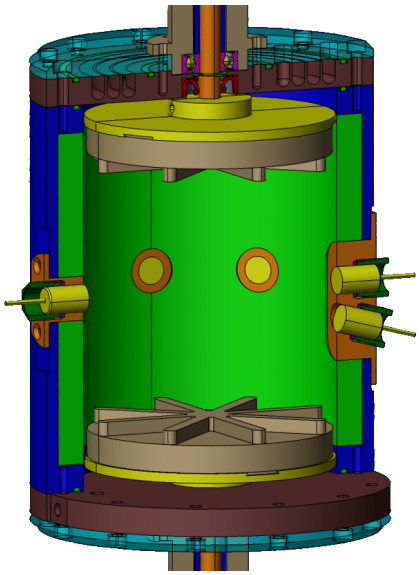

Figure 1: Set-up with transducers.

Table 1: Experimental parameters. $\langle\cdot\rangle$ denotes the ensemble mean and u the velocity fluctuation, a the acceleration. C_ε is assumed to be 0.5. R ist the radius of the cell, H the spacing between the discs. The energy dissipation rate ε is computed according to equation 1.

Aspect ratio cell	$\Gamma = H/2R$	1.1
Temperature water	ϑ	20 °C
Max. angular velocity	Ω_{max}	18.8 rad/s
Reynolds number	$\mathrm{Re} = \Omega_{max} R^2/\nu$	47 000
Microscale Re-number	$\mathrm{Re}_\lambda = \sqrt{15 u_{rms}^4/\varepsilon\nu}$	175 - 225
Kolmogorov length scale	$\eta = (\nu/\varepsilon)^{1/4}$	47 - 60 µm
Kolmogorov time scale	$\tau_\eta = \sqrt{\nu/\varepsilon}$	2.2 - 4.1 ms
Integral length scale	$L = C_\varepsilon u_{rms}^3/\varepsilon$	5.4 - 9.7 mm
Integral time scale	$T = C_\varepsilon u_{rms}^2/\varepsilon$	51 - 75 ms

profiles along emission lines of multiple transducers, recording the velocity component in that direction. We use three transducers in the mid-plane that are arranged in 45 degrees pointing towards the center. This method is able to characterize the flow globally and to detect time dependent flow patterns. The effective time resolution is 62 ms and the spatial resolution is 0.25 mm in the longitudinal and 5-10 mm in the lateral direction.

On the other hand, a custom-built Lagrangian ultrasound measurement technique tracks trajectories of individual tracer particles in the center of the cell. The latter technique is described in detail in Grünberg and Rösgen (2016) and makes use of four transducers covering a volume of approximately $2 \times 2 \times 2\,\mathrm{cm}^3$ in the center of the cell. Here, the transducers are arranged with an angle of 80 degrees to each other in the azimuthal and 15 degrees in the axial direction (figure 1). The flow is insonified with an emission frequency of 2.004 MHz and the echoes of tracer particles are recorded using undersampling at a sampling frequency of 16 kHz. With the parametric frequency estimator 'pmusic' as implemented in MATLAB ® (Schmidt, 1986) the Doppler frequency is estimated for window lengths of 16 samples with 50 percent overlap. This leads to an effective temporal resolution of 0.51 ms, such that the Lagrangian trajectories are spatially and temporally resolved. A Kalman filter allows for the continuous tracking of the trajectories throughout the volume (Borer, 2014).

Doppler techniques measure the velocity $\underline{u}$ via continuous frequency shifts rather than derived from discrete spatial displacements. This allows to compute the acceleration $\underline{a}$ of the fluid flow by a first derivative which is less noise sensitive compared to optical techniques.

In table 1 some main turbulence characteristics for the central region of the cell are listed. These are deduced from the Lagrangian tracking data.

RESULTS

The measurements are analyzed in three major steps. First, we check the agreement between Eulerian and Lagrangian measurements. Second, the influence of different forcings on the large scales is investigated with the UDV data. Finally, the turbulence properties in the center of the cell are examined in detail by making use of the Lagrangian, fully resolved data.

The rms velocity fluctuations from both measurement techniques display a dependence on the variation of the time step dt (figure 2). For the PRBS forcing, an equivalent mean time step as compared to the regular square wave signal can be computed. We use the inverse of the mean frequency of the PRBS spectrum which equals twice the smallest step length, $dt = 2\,dt_{min}$.

For the Eulerian measurements which do not provide all velocity components, we use as an approximation the average of the rms velocity u_{rms} of the radial velocity fluctuations. We average over a range of 1 cm on the side of the converging beam (according to the volume covered by Lagrangian measurements) in the center of the cell utilizing the three channels in the horizontal plane. The scatter of the rms values is of the order of the marker size for both UDV and Lagrangian measurements. The kinetic energy in the center decreases with increasing change rate caused by the flow reversal of the shear cells: The zero-crossing of the disc speed with finite acceleration decreases the absolute energy introduced into the system. More importantly, the dissipation at the blades is increased which reduces the fluid motion induced in the center of the cell. As will be shown later, the slow modes in the center of the cell are progressively suppressed with increasing change rate which leads to a decrease of the energy contained in the large scales (figure 5) and thus a lower rms velocity. The UDV measurements do not capture the true rms velocity since the flow is not fully resolved spatially or temporally and the axial component is neglected. We note that the rms velocities are overestimated compared to the ones from Lagrangian data the more inhomogeneous the flow is, i.e. for slow change rates, as shown below. Discrepancies compared to the Lagrangian data may in part result from the different averaging processes involved. Nevertheless, the UDV observations are qualitatively able to characterize the flow changes.

The radial velocity fluctuations derived from UDV data are used to visualize the macroscopic instabilities we intend to reduce (figure 4). As a mean flow, only a poloidal inward pumping should be present (figure 3). The azimuthal velocity from the shear cells, which we cannot monitor with this measurement technique, should vanish in the transverse plane. With constant forcing (figure 4, top) we clearly see superimposed instabilities which are characterized by a flow reversal in the radial direction and which persist for a significant time. This time-space signature, where the velocity amplitude is plotted over time and radius, can be found with very similar appearance in Miralles (2013), even though their experiments were conducted at higher Reynolds numbers, $Re > 10^6$. Unfortunately, due to their limited measurement possibilities, there is no microscale Reynolds number available for comparison.

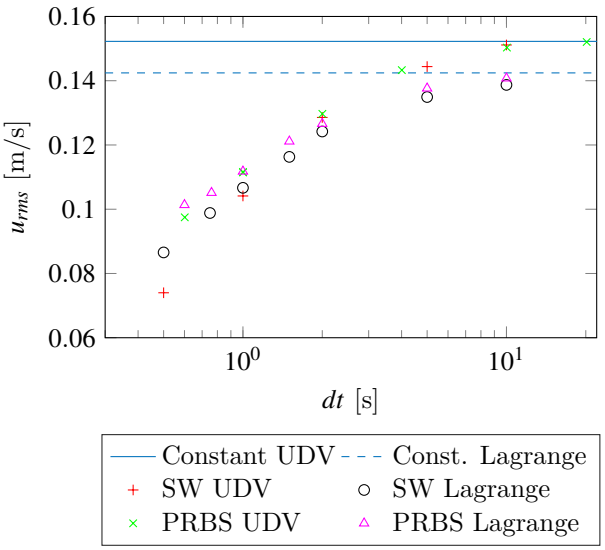

Figure 2: RMS of velocity fluctuations for different forcings.

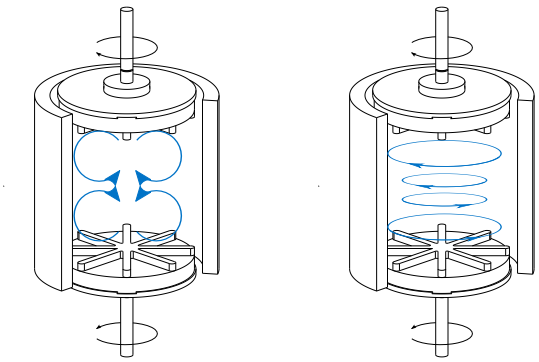

(a) Poloidal pumping. (b) Shearing.

Figure 3: Basic flow modes in a von Kármán cell.

By applying the time-variable forcing, the persistent large-scale phenomena become less pronounced with increasing reversal rates until their appearance is negligible (roughly at $dt = 1-2\,\mathrm{s}$). At very high change rates, only the base flow mode with the poloidal inward pumping remains. The overall radial velocity decreases, too, which is consistent with the reduced rms velocity (figure 2).

This qualitative finding can be translated into a characteristic time scale which is derived from the auto-correlation function of the radial velocity at a position $r = R/2$ from the center, e.g. in the region where the radial mean flow reaches its maximum. We do not use the integral of the auto-correlation function since the data set is not fully converged for large delays due to the relatively long time scales of the slow modes compared to the time series of only about 20 minutes each. Instead, we use a characteristic correlation time $\tau_{1/e}$ defined by the time when the auto-correlation function drops below 1/e. In general, this time scale decreases with increasing change rate which means the low wavenumber modes are ever more suppressed (figure 6). There is a distinct disparity between the time scales of variable and continuous forcing. Apparently, already small variations in the forcing break the very slow modes. These characteristic time scales are two orders of magnitude larger than the estimated integral time scales of the flow of about 51 ms to 75 ms (table 1, small and large time step dt respectively).

At the same location, i.e. at $r = R/2$, the power spectral density

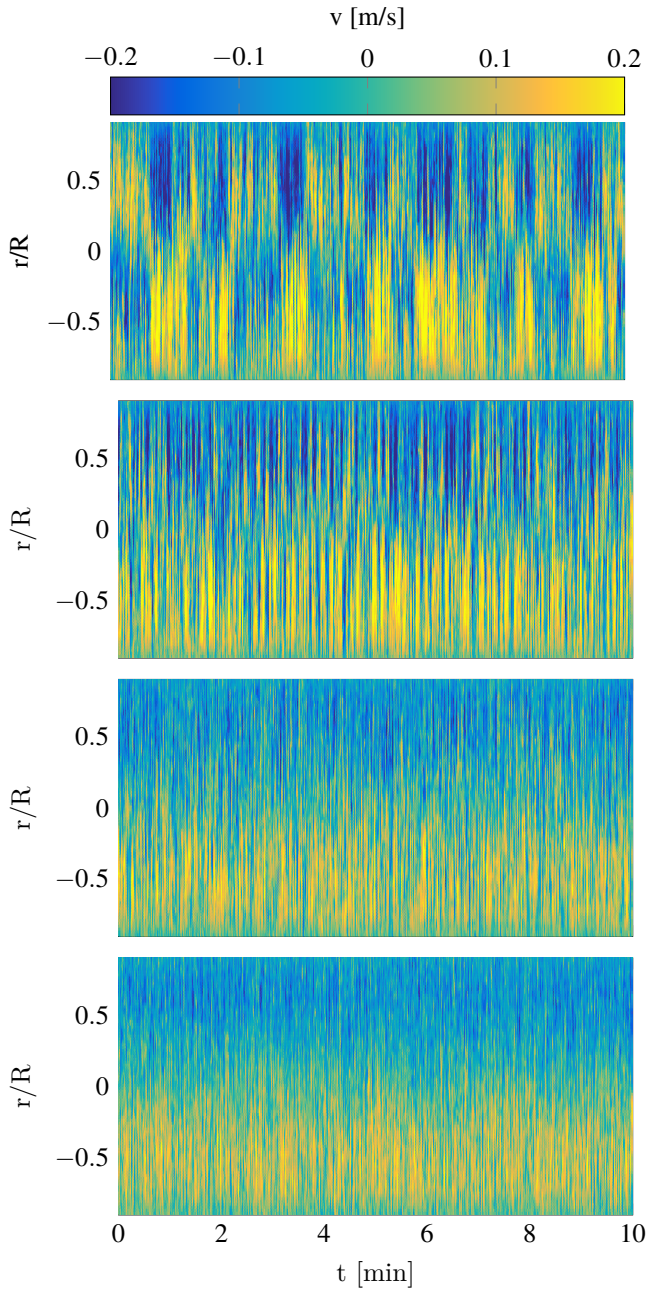

Figure 4: Time-space diagram of radial velocity (UDV measurements). From top to bottom: Constant forcing, square wave forcing with $dt = 5\,\mathrm{s}$, $dt = 1\,\mathrm{s}$ and $dt = 0.5\,\mathrm{s}$.

of the radial velocity fluctuations is computed for different square wave forcings (figure 5). The PRBS measurements behave accordingly, with a little less pronounced cut-off (not shown for the sake of clearness). The fluctuations at large scales are suppressed while the slope of the small scale spectral components remains unchanged. There is a distinct cut-off frequency which varies with the change rate but does not coincide with the forcing frequency. One can identify the forcing frequencies, but their harmonics are no longer visible. This is consistent with the observation that the estimated integral length scales are one order of magnitude lower than the dimensions of the cell such that the direct interference at the blades should not be felt too much in the center of the cell.

Since the global flow field is effectively altered by the changed forcing, it is of interest whether this affects the turbulence properties

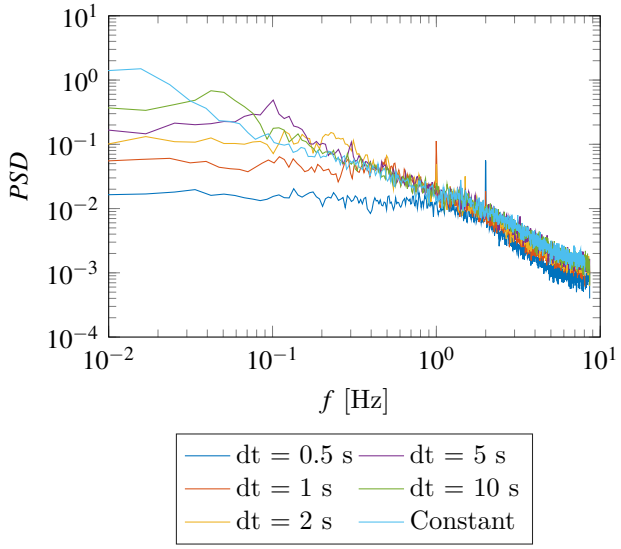

Figure 5: Power spectral density of radial velocity fluctuations from UDV data for SW and constant forcing.

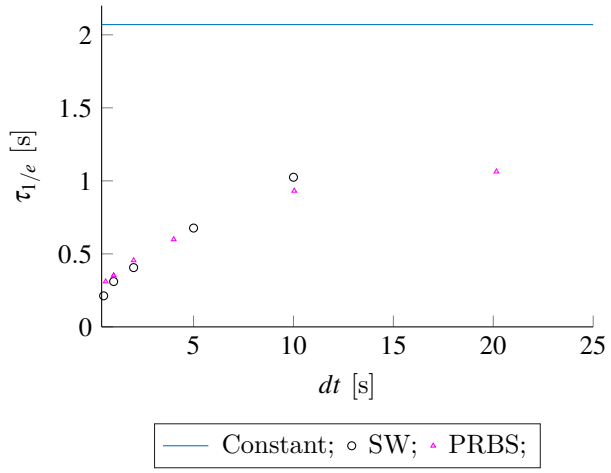

Figure 6: Characteristic auto-correlation time scale of the radial velocity from UDV data.

in the center of the cell.

First, the energy dissipation rate ε is examined (figure 7). It is computed from the trace of the acceleration-velocity covariance tensor, which is valid for decaying, homogeneous turbulence (Mann et al., 1999).

$$\varepsilon = -\langle u_i a_i \rangle \tag{1}$$

The underlying assumptions for validity may not be fully satisfied in our set-up, but the approach is compatible with our measurement technique and generates robust results. The uncertainties, indicated by a dotted line for the constant forcing and error bars for the other cases, are estimated by dividing the data set into subsets and calculating the standard error of the mean. Consistent with the rising Reynolds number for increasing step length dt, the dissipation rate grows. As opposed to the rms velocity, there is a distinct jump from the values for variable to constant forcing. Presumably,

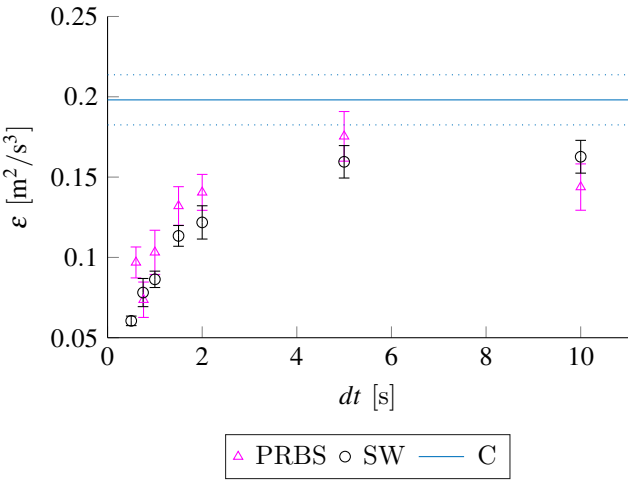

Figure 7: Dissipation rate ε from Lagrangian data.

this is related to the assumption of decaying, globally homogeneous turbulence, which is obviously violated when major flow structures propagate into the center of the cell. This argument is corroborated in the report by Mann et al. (1999) where the dissipation rate is indeed overestimated with this method for a strongly inhomogeneous flow.

Next, we investigate the scaling constant C_0 of the compensated Lagrangian second-order structure function. Due to the lack of a scaling region at our Reynolds number we estimate C_0 based on the peak of the second-order structure function

$$C_0^* = \max\{D_2(\tau)/\tau\varepsilon\} \tag{2}$$

where

$$D_2(\tau) = \left\langle [u(t+\tau) - u(t)]^2 \right\rangle \tag{3}$$

is the second-order structure function and u is one fluctuating velocity component.

In figure 8 the peak C_0^* is plotted after averaging the results of the two transducers in the transversal plane. The uncertainties are computed as above, followed by an error propagation calculation. It can be seen that the maximum of the compensated second order function stays approximately constant within the uncertainties for all reversal rates. This is expected for the small variation of the Taylor microscale Reynolds number. There is an offset between the variable and constant forcing which corresponds to the difference in dissipation rate. The measured values agree roughly with DNS data from Yeung et al. (2006) with the results for variable forcing being closer to the ones computed by Yeung et al. compared to the constant forcing.

Furthermore, the Lagrangian spectrum of the velocity fluctuations is computed via the cosine transform of the auto-covariance function (Sawford and Yeung, 2011) as

$$E = \frac{2}{\pi} \int_0^\infty \langle [u(t+\tau)\, u(t)] \rangle \cos(\omega\tau)\, \mathrm{d}\tau \tag{4}$$

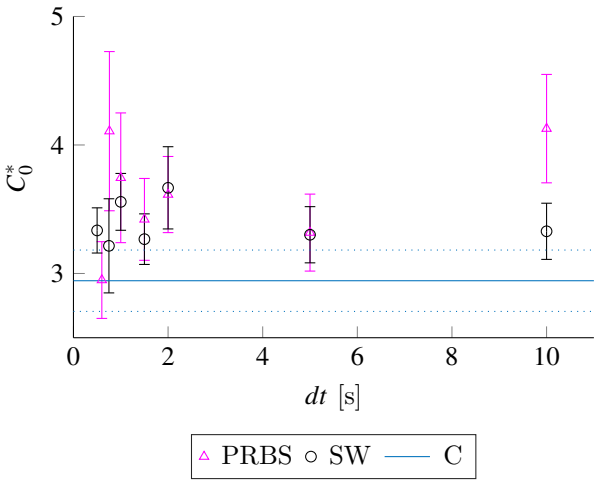

Figure 8: Peak of the second order structure function, C_0^*, from Lagrangian data.

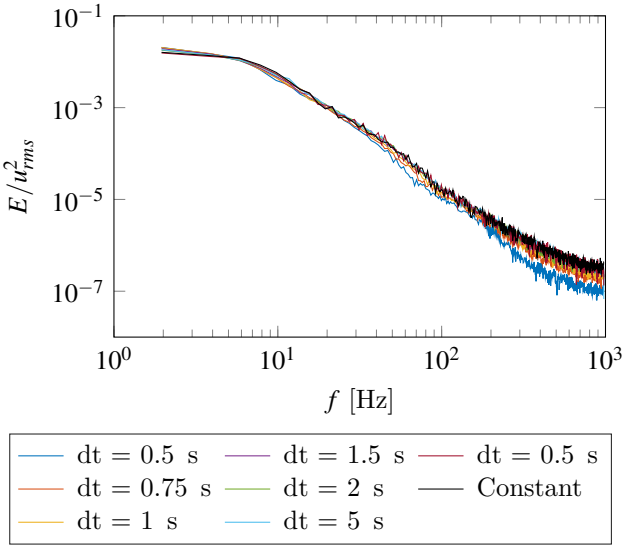

Figure 9: Compensated velocity spectrum for square wave and constant forcing from Lagrangian data.

In figure 9 we see that the normalized energy of the velocity fluctuations remains constant for different forcings (for clarity only the results from SW and constant forcing are plotted). Merely at high wavenumbers, the normalized energy decreases for increasing change rate. The change in the low wavenumbers as in the UDV measurements (figure 5) cannot be observed here due to the limited length of the trajectories. When comparing the frequency range of the two spectra, the Lagrangian spectrum is cut off approximately at the frequency where the differences become visible.

Higher order moments of the velocity fluctuations in the different directions are an indicator for the isotropy of the turbulence in the center. With the flow reversal we enhance a radially inward pumping mode and reduce the azimuthal flow. It is still expected that transversal and axial directions differ, which is confirmed in figure 10, where the skewness and kurtosis of the velocity fluctuations are plotted over time step. In contrast, anisotropies for example from inevitable small inhomogeneities of the flow cell in the transversal plane are reduced with increasing change rate and the skewness approaches zero (figure 10a). At the same time, the kurtosis (figure 10b) is increased from sub-Gaussian behavior for the transversal components and even further increased for the axial component. In homogeneous, isotropic turbulence we would expect Gaussian behavior which is not observed as a result of the modified forcing. We have to note, though, that these assumptions are never met in the center of the cell.

CONCLUSION

The slow flow modes appearing in von Kármán flow cells could be destroyed successfully without degrading the turbulence properties in the center of the cell. In order to achieve this, random and regular change of the disc rotation sense (square wave or PRBS forcing respectively) has been applied. Both square wave or PRBS forcing with time steps around $dt = 2$s proved to be a good compromise between effectively altering the global flow while retaining comparatively high Reynolds numbers. It is remarkable that both forcing methods yield very similar results. Nevertheless, the destruction of higher order flow modes reduces the micro scale Reynolds numbers in the center of the cell. A solution to prevent this may be the increase of the disc rotation speed while maintaining the reversal rates.

The Doppler ultrasound velocity profiles show a clear frequency cut-off in the velocity spectrum and a decrease of the correlation time whereas Lagrangian tracking of tracer particles confirmed the robustness and slight improvement of turbulence features in the cell center, namely the peak of the compensated second order structure functions, the velocity spectrum or higher order moments.

It appears now possible to investigate the dependence of turbulence characteristics due to modifications of the fluid properties or in a magneto-hydrodynamic flow without a direct or indirect influence of dominant eddies. The exclusive presence of only the lowest order pumping mode, namely the radial inward flow in the central plane, facilitates the establishment of a controlled reference flow compared to the constant forcing case.

References

Borer, D. J. 2014 4D flow visualization with dynamic vision sensors. *ETH Zürich* .

Chien, C.-C., Blum, D. B. and Voth, G. A. 2013 Effects of fluctuating energy input on the small scales in turbulence. *Journal of Fluid Mechanics* **737**, 527–551.

Cortet, P.-P., Diribarne, P., Monchaux, R., Chiffaudel, A., Daviaud, F. and Dubrulle, B. 2009 Normalized kinetic energy as a hydrodynamical global quantity for inhomogeneous anisotropic turbulence. *Physics of Fluids* **21** (2), 025104.

Douady, S., Couder, Y. and Brachet, M. E. 1991 Direct observation of the intermittency of intense vorticity filaments in turbulence. *Physical Review Letters* **67** (8), 983.

Grünberg, T. and Rösgen, T. 2016 Turbulent flow of a fluid with anisotropic viscosity. *Journal of Fluid Mechanics* **792**, 252–273.

Mann, J., Ott, S. and Andersen, J. S. 1999 Experimental study of relative, turbulent diffusion.

Maurer, J., Tabeling, P. and Zocchi, G. 1994 Statistics of turbulence between two counterrotating disks in low-temperature helium gas. *EPL (Europhysics Letters)* **26** (1), 31.

Miralles, S. 2013 Etudes expérimentales de l'instabilité dynamo: mécanismes de génération et saturation. *Ecole Normale Supérieure de Lyon-ENS LYON* .

Nore, C., Tartar, M., Daube, O. and Tuckerman, L. S. 2004 Survey of instability thresholds of flow between exactly counter-rotating disks. *Journal of Fluid Mechanics* **511**, 45–65.

Ravelet, F., Marié, L., Chiffaudel, A. and Daviaud, F. 2004 Multistability and memory effect in a highly turbulent flow: Experi-

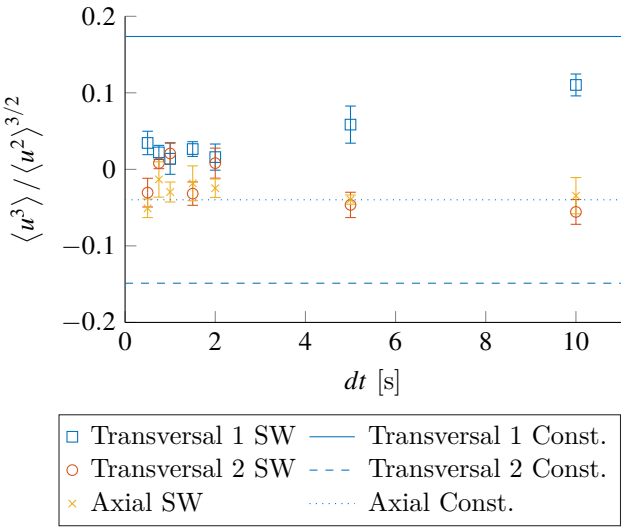

(a) Skewness.

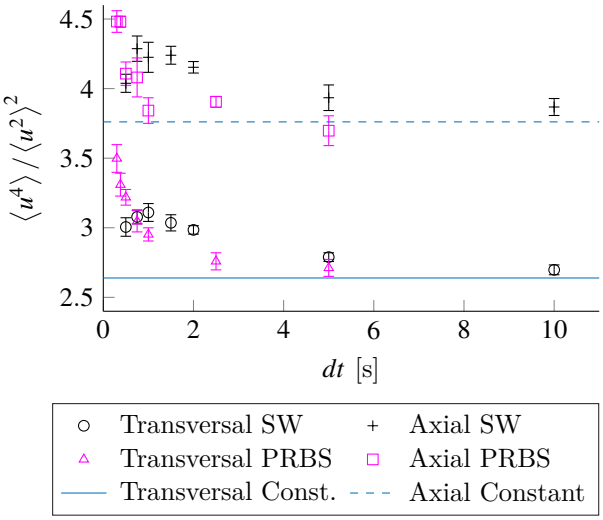

(b) Kurtosis. Transversal directions are avaraged.

Figure 10: Skewness and kurtosis of PDF of velocity fluctuations from Lagrangian data. The error bars for constant forcing are not shown for clarity but have the same order of magnitude as those for the variable forcing.

mental evidence for a global bifurcation. *Physical Review Letters* **93** (16).

Saint-Michel, B., Dubrulle, B., Marié, L., Ravelet, F. and Daviaud, F. 2014 Influence of Reynolds number and forcing type in a turbulent von Kármán flow. *New Journal of Physics* **16** (6), 063037.

Sawford, B. L. and Yeung, P. K. 2011 Kolmogorov similarity scaling for one-particle Lagrangian statistics. *Physics of Fluids* **23** (9), 091704.

Schmidt, R. O. 1986 Multiple emitter location and signal parameter estimation. *IEEE Transactions on Antennas and Propagation* **AP-34** (3), 276–280.

de la Torre, A. and Burguete, J. 2007 Slow dynamics in a turbulent von Kármán swirling flow. *Physical Review Letters* **99** (5).

Voth, G. A., La Porta, A., Crawford, A. M., Alexander, J. and Bodenschatz, E. 2002 Measurement of particle accelerations in fully developed turbulence. *Journal of Fluid Mechanics* **469**.

Yeung, P. K., Pope, S. B. and Sawford, B. L. 2006 Reynolds number dependence of Lagrangian statistics in large numerical simulations of isotropic turbulence. *Journal of Turbulence* **7**, N58.